Quasiparticle band offset at the (001) interface and band gaps in ultrathin superlattices of GaAs-AlAs heterojunctions

S. B. Zhang,* Marvin L. Cohen, Steven G. Louie, and D. Tománek†
Department of Physics, University of California, Berkeley, Berkeley, California 94720
and Materials and Chemical Sciences Division, Lawrence Berkeley Laboratory, Berkeley, California 94720

Mark S. Hybertsen
AT&T Bell Laboratories, 600 Mountain Avenue, Murray Hill, New Jersey 07974-2070
(Received 27 December 1989)

A newly developed first-principles quasiparticle theory is used to calculate the band offset at the (001) interface and band gaps in 1×1 and 2×2 superlattices of GaAs-AlAs heterojunctions. We find a sizable many-body contribution to the valence-band offset which is dominated by the many-body corrections to bulk GaAs and AlAs quasiparticle energies. The resultant offset $\Delta E_v=0.53\pm0.05$ eV is in good agreement with the recent experimental values of 0.50–0.56 eV. Our calculated direct band gaps for ultrathin superlattices are also in good agreement with experiment. The X_{1c}-derived state at point $\bar{\Gamma}$, is however, above the Γ_{1c}-derived state for both the 1×1 and 2×2 lattices, contrary to results obtained under the virtual-crystal approximation (a limiting case for the Kronig-Penny model) and some previous local-density-approximation (corrected) calculations. The differences are explained in terms of atomic-scale localizations and many-body effects. Oscillator strengths and the effects of disorder on the spectra are discussed.

I. INTRODUCTION

Because of their great importance in high-speed electronic devices, semiconductor heterojunctions have received considerable attention.[1–4] One of the fundamental problems for these systems is the determination of their electronic structure and band offsets. Contrary to earlier belief,[5–10] relatively larger valence-band offsets are now generally accepted.[11–15] A 65/35 ratio was found for the conduction (ΔE_c) and valence (ΔE_v) -band offsets of the prototypical GaAs-AlAs heterojunction grown with a molecular-beam-epitaxy (MBE) technique. Considerable theoretical effort has been made to predict these offsets.[9–11,16–22] Earlier theories[9–11] predicted a nearly vanishing value for the valence-band offset for the GaAs-AlAs heterojunction, except for an empirical-pseudopotential calculation.[16] Recently, local-density-functional (LDA) calculation using *ab initio* pseudopotentials gave $\Delta E_v=0.37$ eV.[18] All-electron calculations within LDA also predicted a large valence-band offset.[19,20] The discrepancies between the earlier models and recent calculations are now understood.[20] The earlier (tight-binding-type) models had omitted the *d* core levels. In *ab initio* pseudopotential calculations, the interaction between the *d* core and valence electrons is included through nonlocal *d* potentials although the cores are frozen at the atomic level.[23]

An area closely related to the heterojunction is the study of superlattices. A superlattice is a periodic array of heterojunctions. High-quality superlattices of artificial periods can be made using the MBE technique.[24] With the recent development of the metalorganic chemical vapor deposition (MOCVD) technique, ultrathin GaAs/AlAs (001) superlattices down to 1×1 period are also available.[25] New physical phenomena related to quantum confinement, Brioullin-zone folding, and quasi-two dimensional electron-gas behavior occur within the superlattices. Superlattices therefore have potential applications. A perturbative envelope-function approach (or Kronig-Penney model) proposed by Bastard is often used to describe large-period superlattices.[26,27] The sophisticated LDA calculations currently are only applicable to ultrathin superlattices.[28–36]

However, the use of the LDA eigenvalues can lead to grossly incorrect predictions for the band gaps as well as for the band offsets. Such errors, although they do not diminish the merits of the Hohenberg-Kohn-Sham LDA in correctly determining ground-state properties of solids, reflect the inability of this approach to calculate the electronic structure of excited states. Because of this inability, LDA results for superlattice electronic structure, which are believed to be more erroneous than band offsets, are usually cross checked by other methods or experiments, e.g., although most recent LDA calculations predict that the lowest-folded *X* state at point Γ is above the Γ-derived state for the 1×1 and 2×2 lattices, this result is not generally accepted since it appears to contradict with experimental results for larger lattice periods[37–40] and the classical envelope-function results.[26,27] Often, the LDA results are "corrected" by adding the known LDA errors for the band gaps in bulk materials [we shall refer to these as LDA (corrected) results]. An underlying assumption for these corrections is that many-body effects going beyond the LDA are independent of the superlattice periods. An adequate approach to the excitation energies and band gaps is to

solve the self-energy equation[41] for quasiparticle energies. We have recently extended Hedin's *GW* quasiparticle formalism[42] for the self-energy operator to systems without an inversion center.[43] Here, this formalism is applied to the GaAa-AlAs heterojunction band offset and band gaps in ultrathin superlattices.

The paper is organized as follows. In Sec. II, we present a theory for valence-band offset and its application to GaAs-AlAs heterojunctions. In Sec. III, the electronic structures of the 1×1 and 2×2 superlattices of GaAs/AlAs (001) are discussed. A brief summary is given in Sec. IV.

II. GaAs/AlAs (001) VALENCE-BAND OFFSET

The LDA calculations for semiconductors and semiconductor interfaces have the important advantage that the self-consistent charge densities are properly calculated. Thus these calculations provide the correct dipoles at the interfaces. However, using the LDA to calculate the valence-band offset further requires that the LDA eigenvalues representing the position of the valence-band edge states in the materials on both sides of the interface adequately approximate the true electron-removal energies, i.e., the quasiparticle valence-band edges. This assumption is found to be incorrect and the many-body correction to the LDA valence-band offset is significant. We find this correction to be 0.12 ± 0.02 eV for the AlAs/GaAs (001) interface; this is about 30% of the LDA offset value ($\Delta E_v^{\rm LDA}=0.41$ eV). Hence, our calculated value for the valence-band offset is $\Delta E_v=0.53\pm0.05$ eV in good agreement with the most recent experimental values of 0.53–0.56 eV.[14,15]

Within the quasiparticle framework, the valence-band offset can be rigorously written as the difference between the quasiparticle valence-band maxima at each side of the materials far away from the boundary

$$\Delta E_v = E^{\rm qp}_{\rm VBM,GaAs} - E^{\rm qp}_{\rm VBM,AlAs} \ . \tag{1}$$

Following the procedure used to derive Eq. (22) in Ref. 43, this can be written as

$$\Delta E_v = \Delta E_v^{\rm LDA} + \delta'^{\rm int}_{\rm VBM} + \delta_{\rm VBM} \ , \tag{2}$$

with $\Delta E_v^{\rm LDA}$ defined to be the LDA valence-band offset,

$$\begin{aligned}\delta'^{\rm int}_{\rm VBM} &= (V_H^{\rm GaAs} - V_H^{\rm AlAs}) - (V_H^{\rm GaAs} - V_H^{\rm AlAs})^{\rm LDA} \\ &= V_d(\rho) - V_d(\rho^{\rm LDA}) \ ,\end{aligned} \tag{3}$$

and

$$\delta_{\rm VBM} = (\Sigma - V_{\rm xc})^{\rm VBM}_{\rm GaAs} - (\Sigma - V_{\rm xc})^{\rm VBM}_{\rm AlAs} \ , \tag{4}$$

where V_H denotes the Hartree energy, $\langle\psi_{\rm VBM}|\hat{V}_H(\rho)|\psi_{\rm VBM}\rangle$; V_d is the interfacial electrostatic dipole potential, ρ and $\rho^{\rm LDA}$ are the exact and the LDA charge densities; and Σ and $V_{\rm xc}$ denote the expectation values, $\langle\psi_{\rm VBM}|\hat{\Sigma}(E^{\rm qp}_{\rm VBM})|\psi_{\rm VBM}\rangle$ and $\langle\psi_{\rm VBM}|\hat{V}_{\rm xc}|\psi_{\rm VBM}\rangle$, respectively. Here, $\hat{\Sigma}$ is the self-energy operator, while $\hat{V}_{\rm xc}$ is the density-functional exchange-correlation potential, evaluated in the LDA.

The dipole correction $\delta'^{\rm int}$ is from corrections to the Hartree energies V_H, which is expected to be small. This term will, however, be examined later since it has not been shown that using LDA to approximate the exact charge densities does not cause sizable error in the electrostatic dipole. The many-body correction term $\delta_{\rm VBM}$, is, on the other hand, a bulk property since the offset should be evaluated at large distances away from the interface and both operators $\hat{\Sigma}$ and $\hat{V}_{\rm xc}$ are short range.

To calculate the LDA band offset $\Delta E_v^{\rm LDA}$ we use an approach similar to that in Ref. 16 and of Van de Walle and Martin.[44] The local part of the self-consistent LDA potential of supercells, $V(\mathbf{r})$ is averaged within a volume equal to the bulk unit cell in the bulklike regions of GaAs and AlAs. The average potential is denoted here as $\bar{V}$ and their difference $\Delta\bar{V}=\bar{V}_{\rm GaAs}-\bar{V}_{\rm AlAs}$ is used to line up bulk LDA eigenvalues. In this calculation, the GaAs lattice constant ($a_0=5.6523$ Å) (Ref. 45) is used corresponding to a MBE-grown heterojunction on a GaAs substrate. The values of the LDA valence-band maxima converged to within 0.02 eV which in our estimate will cause an uncertainty of 5 meV in the result for the LDA valence-band offset. The relative position of the average potentials $\bar{V}$ is calculated using results from 2×2 and 3×3 lattices and a 6-$\bar{\mathbf{k}}$-point set for the Brillouin-zone sum.[46] An energy cutoff of 12 Ry is used for the plane-wave expansion in the supercell calculation. The energy cutoffs, the number of $\mathbf{k}$ points, and the layer thickness of the supercells ensure a total convergence to within 0.02 eV. The calculations were iterated until the potential was self-consistent to within 10^{-5} Ry in the whole space and $\Delta\bar{V}$ was stable within a few meV. Hence, our result for the LDA valence-band offset after taking into account the spin-orbit splittings is $\Delta E_v^{\rm LDA}=0.41\pm0.03$ eV. A slightly different scheme for evaluating the LDA band offset[47] has recently been proposed. As long as the $\Delta\bar{V}$ is converged with respect to the layer thickness in the superlattice, the two schemes yield similar results.

We estimate the dipole correction $\delta'^{\rm int}_{\rm VBM}$ in the following way. V_d in Eq. (3) is the electrostatic dipole potential and hence is independent of the band and $\mathbf{k}$- vector indices as well as the spatial variables. We can calculate V_d by taking the difference between the average Hartree potentials in the bulklike GaAs and AlAs regions. The average is with respect to the x and y coordinates, and with respect to the z coordinate within bulk period. Hence,

$$V_d = \frac{6e^2L^2}{\pi^2 V_{\rm cell}}[\rho^r(0,0,1) - \sqrt{3}\rho^i(0,0,1) + \cdots] \ , \tag{5}$$

where e is the electron charge, L and $V_{\rm cell}$ are the cell size (along supercell axis z), and the volume of the supercell used to evaluate V_d, $\rho^r(\mathbf{G})$, and $\rho^i(\mathbf{G})$ are the real and imaginary parts of the number charge density (in units of electrons per supercell), respectively. The supercell used here is a 3×3 cell. One should notice that although V_d is a well-defined quantity, some minor details of Eq. (5) depend on the choice of origin. The higher-order terms of Eq. (5) have the form

$$\rho(0,0,(2n+1))/(2n+1)^3, \quad n=1,2,3,\ldots,$$

TABLE I. The many-body correction δ_{VBM} versus number of q points used in the Brillouin-zone sum.

N_q	3	10	14
δ_{VBM} (eV)	0.082	0.116	0.121

so that the series converges quickly. This is because the higher Fourier components of charge density have more spatial oscillations and hence are less effective in terms of transferring charge across the boundary. About 80% of the electrostatic dipole is determined by the lowest **G** component of charge, $\mathbf{G}=(0,0,1)$, which is least affected by the LDA used to approximate the short-range exchange-correlation potentials. In general, the low-**G** components of the LDA charge density agree with experiment to within a few percent. Moreover, from the linear dependence of V_d on charge density ρ and $V_d^{\mathrm{LDA}}=-0.36$ eV for GaAs/AlAs (001), we estimate that a 1% deviation in the low **G** components of the LDA charge density from the exact density-functional result affects V_d by less than 4 meV. Hence, δ'^{int} is negligible.

The bulk many-body term δ_{VBM} is determined as follows. In Table I δ_{VBM} is given as a function of the number of q points, N_q used in the Brillouin-zone sum in Eqs. (24) and (25) of Ref. 43 for evaluating Σ. The numerical value of δ_{VBM} is 0.12 eV for $N_q=14$ and the estimated accuracy is about 10 meV. A systematic trend for the valence band is easily observed in Fig. 1 in which $E_{n\mathbf{k}}^{qp}-\epsilon_{n\mathbf{k}}^{\mathrm{LDA}}$ versus $E_{n\mathbf{k}}^{qp}$ is shown for both the GaAs and AlAs p-like valence bands. There is a consistent 0.1–0.2 eV difference in the many-body correction to the LDA eigenvalues for the GaAs and AlAs valence-band states. This is consistent with the value of the many-body contribution to the valence-band offset δ_{VBM}, which is determined to be 0.12 ± 0.02 for this interface. This contribution is significant and is about 30% of the LDA value.

The sign of δ_{VBM} can be understood by examining the individual terms of the self-energy at the valence-band maxima: the bare exchange, screened exchange, and Coulomb-hole components (see Table II). A more negative bare-exchange energy is found in AlAs, which is 0.3 eV lower than that of GaAs. The exchange hole for this state in AlAs is therefore deeper and narrower than that in GaAs. This is consistent with a more localized valence-band wave function for AlAs. The occupied p-like band of AlAs is found to be about 1.1 eV narrower than that of GaAs. The screened exchange term reduces the bare exchange in both GaAs and AlAs but has little effect on their difference. However, the Coulomb-hole energy competes with the exchange energy and reduces the differences by about 0.2 eV. A larger negative-

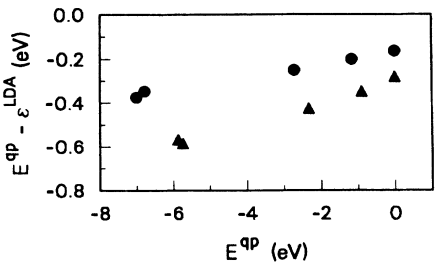

FIG. 1. Quasiparticle correction $E_{n\mathbf{k}}^{qp}$-$\epsilon_{n\mathbf{k}}^{\mathrm{LDA}}$ vs quasiparticle energy $E_{n\mathbf{k}}^{qp}$ for the p-like valence bands of bulk GaAs (solid circles) and AlAs (solid triangles). $E_{n\mathbf{k}}^{qp}=0$ corresponds to the top of the valence band.

Coulomb-hole energy in GaAs is consistent with more effective screening [$\epsilon_{\infty,\mathrm{GaAs}}=10.9$ and $\epsilon_{\infty,\mathrm{AlAs}}=8.16$ (Ref. 45)]. Since LDA gives an almost identical exchange-correlation potential V_{xc} for GaAs and AlAs, the many-body correction to the LDA is more negative in AlAs; this leads to a positive δ_{VBM}. This conclusion agrees with previous results for diamond, Si, Ge, and LiCl, where the many-body correction to the valence-band maximum increases as the wave functions become more localized.[42]

In conclusion, the LDA cannot be used for an accurate prediction of the band offsets although it is a useful method for many ground-state properties. We expect that the many-body effects will play a more important role in band offsets for chemically less similar materials.

III. GaAs/AlAs (001) ULTRATHIN SUPERLATTICES

Recent experiments show that ultrathin superlattices exhibit high degrees of crystalline order, small interlayer diffusion, and hence are metastable. This has stimulated many studies on their electronic structures.[26–36,48–60] It is expected that these structures have different electronic properties than thick-layer superlattices. In this section, we apply the quasiparticle theory to the electronic structures of the 1×1 and 2×2 superlattices and discuss special features of these lattices such as atomic-scale localization, avoided band crossings, effective-mass change, anisotropic oscillator strength, and the degeneracy of segregating states.

The calculational details can be found in Ref. 43. In particular, a 16-Ry cutoff energy (for the 1×1 lattice) and a 12-Ry cutoff energy (for the 2×2 and 3×3 lattices) in the plane-wave expansion are used for the LDA self-consistent potentials. A 16-Ry cutoff energy is used throughout to obtain the LDA eigenvalues and wave functions. To calculate Σ, 250 and 500 bands have been

TABLE II. The bare exchange Σ_x, screened exchange Σ_{sex}, Coulomb hole Σ_{coh}, self-energy Σ, and the LDA exchange-correlation potential V_{xc} at the valence-band maximum for GaAs and AlAs in eV.

	Σ_x	Σ_{sex}	Σ_{coh}	Σ	V_{xc}
GaAs	−12.638	8.987	−8.280	−11.931	−11.759
AlAs	−12.936	8.992	−8.110	−12.054	−11.761

used for the 1×1 and 2×2 lattices, respectively. Up to 11 **q** points in an irreducible zone of the superlattice have been used for the Brillouin-zone sum for the 1×1 lattice. The sum over *umklapp* process was truncated at $G^2_{\max}=9.0$ Ry. The error due to these finite cutoffs is estimated to be about 0.1 eV. For the 2×2 lattice, six **q** points are used for the Brillouin-zone sum and the sum over *umklapp* process has been truncated at $G^2_{\max}=7.84$ Ry. The lattice constant of GaAs ($a_0=5.6523$ Å) (Ref. 45) is used for the superlattice. A 0.14% mismatch of the lattice constant ($a_0=5.660$ Å) (Ref. 45) may cause some relaxation but this should not affect the band structure significantly.[49]

A. Band structures of 1×1 and 2×2 lattices

The unit cell of the 1×1 lattice and the corresponding Brillouin zone are shown in Fig. 2. The 1×1 Brillouin zone can be obtained by folding the bulk zone once. Hence, point $\bar{\Gamma}$ corresponds to both points Γ and X_z, point $\bar{M}$ corresponds to both points X_x and X_y, and point $\bar{R}$ corresponds to both points L_z and L_{-z} of the corresponding bulk Brillouin zone, respectively. For a 2×2 lattice, each $\bar{\mathbf{k}}$ point corresponds to the folding of four **k** points of the zinc-blende-structure lattice. Hence, point $\bar{\Gamma}$ is given by points Γ, X_z, and $\pm\Delta/2$; point $\bar{M}$ by points $X_{x,y}$ and $W_{y-z,x-z}$; and point $\bar{X}$ by points $L_{\pm z}$ and $\pm\Sigma/2$, respectively. The 1×1 and 2×2 lattices belong to different space groups. This gives rise to symmetry oscillations with respect to layer thickness for zone-folded states.

The calculated quasiparticle band structures are shown in Figs. 3(a) and 3(b) along the symmetry line $\bar{R}-\bar{\Gamma}-\bar{M}$ (1×1) and $\bar{X}-\bar{\Gamma}-\bar{M}$ (2×2), respectively. For an accurate band structure for Ga(Al)-As, the spin-orbit splitting should be included. These splittings for ultrathin superlattices have not been measured accurately so that no experimental data can be used to "refine" current theoretical nonspin-orbit results. We have calculated the spin-orbit splittings with the LDA. The many-body corrections are then included according to the linear combination of superlattice states induced by the spin-orbit interaction. An alternative approach is to calculate the spin-orbit interaction for the quasiparticle states. The results between the two approaches are, however, quite similar (less than 0.01 eV difference for the GaAs-AlAs heterojunction). We determine the split-off gap at the valence-band maximum for the 1×1 lattice to be 0.34 eV.

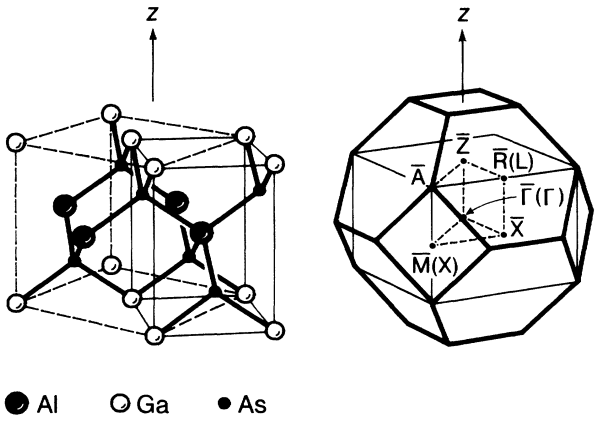

FIG. 2. The conventional and primitive unit cells of the 1×1 GaAs/AlAs superlattice along the [001] direction and the corresponding Brillouin zone drawn within an fcc zone.

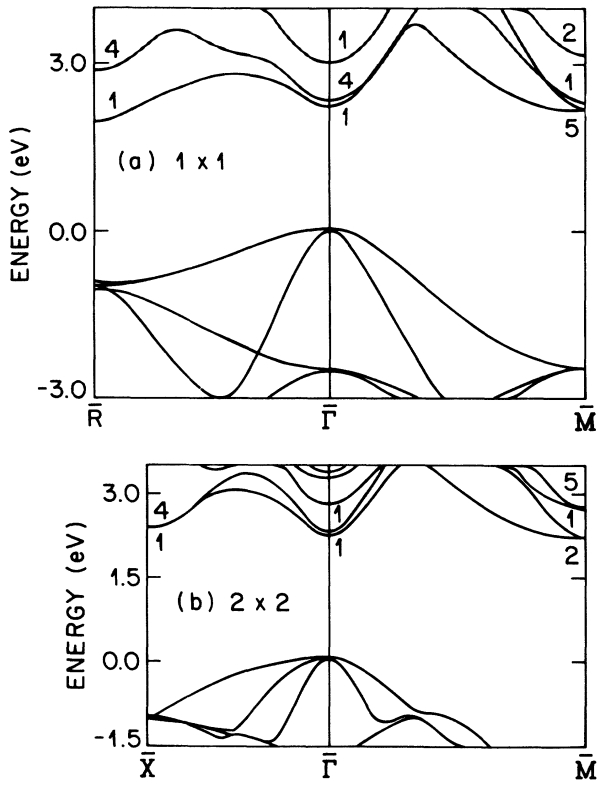

FIG. 3. Quasiparticle band structures in the vicinity of the gap (a) for the 1×1 lattice along the symmetry line $\bar{R}-\bar{\Gamma}-\bar{M}$; (b) for the 2×2 lattice along the symmetry line $\bar{X}-\bar{\Gamma}-\bar{M}$. Spin-orbit splittings are not included.

The effects of core-valence exchange should also be considered. These effects are small but are important for predicting accurate energy gaps as discussed in Refs. 42 and 43. The core-valence effects are in principle very short in range and should be nearly identical for bulk and for superlattices. Hence, by adding these terms, the calculated energy levels for the superlattices should be closer to the true values and are hence more reliable. Because of the absence of compatible and accurate all-electron quasiparticle calculations for GaAs and AlAs, the differences between the experimental data and present quasiparticle values for bulk GaAs and AlAs will be used as the core corrections for the superlattices.[61] The weighting factors used in the correction for dividing bulk regions are determined by integrating the charge density over the GaAs region (see Table III). The major effect of the core-valence exchange is to move the lowest $\bar{\Gamma}_{1c}$ state up relative to other conduction-band states by about 0.2 eV.

We would like to emphasize the difference between the present procedure of considering core effects and the

TABLE III. Total charge integrated over GaAs region for some symmetry states for 1×1, 2×2, and 3×3 lattices in percentage (%). Data are shown with bulk symmetries.

(bulk)	Γ_{1c}	$X_{1c,z}$	L_{1c}	$X_{1c,xy}$
1×1	65	54	40	47
2×2	56	44	59	42
3×3	61	26		

LDA (corrected) methods. The core correction has a well-established physical origin and is small compared with the gap value (about $\frac{1}{10}$ of the gap value or less). In contrast, in the LDA (corrected) cases, the correction terms are large with the entire many-body effect taken as a frozen term from the bulk characters of the states. Without the present quasiparticle calculation, it would be impossible to estimate the magnitude of the errors in the LDA (corrected) calculations.

Present results including the spin-orbit interactions as well as the core effects are given in Table IV. We estimate a total uncertainty of about 0.1 eV for these results. A few features should be pointed out.

For the 1×1 lattice, (1) the $\bar{\Gamma}_{1c}(\Gamma_{1c})$ state is below the $\bar{\Gamma}_{4c}(X_{1c,z})$ state; (2) the $\bar{R}_{1c}(L_{1c})$ state is the conduction-band minimum; (3) the $\bar{M}_{5c}(X_{1c,xy})$ state is lower than the $\bar{\Gamma}_{4c}(X_{1c,z})$ state.

For the 2×2 lattice, (1) the $\bar{\Gamma}_{1c}(\Gamma_{1c})$ state is still below the $\bar{\Gamma}_{1c}(X_{1c,z})$ state, but the energy separation is slightly reduced; (2) the low-lying L-derived state $\bar{X}_{1c}$ is no longer the conduction-band minimum and is, instead, above the $\bar{\Gamma}_{1c}$ and $\bar{M}_{2c}$ states; (3) the conduction-band minimum is at the $\bar{M}_{2c}(X_{1c,xy})$ state.

The LDA (corrected) results are also given in Table IV. The results of Wei and Zunger agree better with the present results, while the results of Ref. 31 are consistently smaller. Contrary to the quasiparticle results, the LDA (corrected) calculations state that the Γ_{1c}-derived state is above the $X_{1c,z}$-derived state. This is partly because the estimated many-body corrections for the folded X state used in the LDA (corrected) calculations are inaccurate. We find that the calculated many-body corrections for the 1×1 lattice are 0.91 eV for $\bar{\Gamma}_{2c}(\Gamma_{1c})$, 0.86 eV for $\bar{\Gamma}_{4c}(X_{1c})$, and 0.79 eV for $\bar{M}_{5c}(X_{1c})$. In contrast, the mean values of the many-body corrections for GaAs and AlAs (Ref. 43) are 0.92 eV (Γ_{1c}), and 0.77 eV (X_{1c}), respectively. These mean values are implicitly used in the LDA (corrected) calculations. We notice a sizable difference between our result (2.23 eV) and Wei and Zunger's result (2.02 eV) for the $\bar{\Gamma}_{1c}(X)$ state for the 2×2 lattice. Performing an LDA (corrected) calculation similar to Wei and Zunger, we get 2.18 eV for this state. Hence, this particular discrepancy is not caused by many-body corrections. Since for the 2×2 lattice both the Γ and the folded X states have $\bar{\Gamma}_1$ symmetry and hence mix with each other, convergence in the calculation is perhaps crucial. We point out that for a nonconverged calculation with an energy cutoff of 12 Ry, the pseudodirect quasiparticle gap would be smaller than the direct band gap, the reverse of our more converged results.

TABLE IV. Quasiparticle energies from the top of valence band for symmetry points for 1×1 and 2×2 lattices in eV. Core corrections and spin-orbit splittings have been considered. LDA (corrected) and virtual-crystal-approximation (VCA) results are also given.

1×1	$\bar{\Gamma}_{1c}$	$\bar{\Gamma}_{4c}$	$\bar{R}_{1c}$	$\bar{M}_{5c}$
present	2.11	2.23	1.85	2.13
WZ[a]	2.18	2.17	1.88	2.10
GCC[b]	1.93	1.99	1.69	
2×2	$\bar{\Gamma}_{1c}$	$\bar{\Gamma}_{1c}$	$\bar{X}_{1c}$	$\bar{M}_{2c}$
present	2.18	2.23	2.34	2.16
WZ[a]	2.23	2.02	2.35	2.06
GCC[b]	2.03	1.85		
(bulk)	Γ_{1c}	$X_{1c,z}$	L_{1c}	$X_{1c,xy}$
VCA	2.32	2.13	2.32	2.13

[a]Reference 29.
[b]Reference 31.

The virtual-crystal-approximation (VCA) results for $Ga_{0.5}Al_{0.5}As$ alloy are also shown in Table IV for comparison with the quasiparticle calculation for the 1×1 lattice. These results are obtained in the following way. The VCA energy gaps have been found within the LDA to change nearly linearly with respect to the change of cation composition x.[50] Hence, we have used here an empirical approach and list in Table IV the arithmetic average of the measured GaAs and AlAs band gaps as the VCA results for $x=0.5$. Such a VCA is a special case of the Kronig-Penny model for zero well and barrier thicknesses. The quasiparticle gap for $X_{1c,xy}$-derived states (2.13 eV) agrees well with the VCA result (2.13 eV). The gap for the $\bar{\Gamma}_{4c}(X_{1c,z})$ state (2.23 eV) is, however, 0.1 eV higher because of an increase in the many-body correction discussed earlier and a repulsion from the lower Γ-derived $\bar{\Gamma}_{4v}$ valence state. For the L_{1c}-derived state, the quasiparticle gap (1.85 eV) is smaller than the VCA result (2.32 eV) because of a strong repulsion between the two originally degenerate L_{1c} states. The average value of 2.32 eV for the two repelling states, 1.85 and 2.79 eV, is on the other hand, in reasonable agreement with the VCA. The most significant difference is of the Γ_{1c}-derived state for which the quasiparticle gap (2.11 eV) is about 0.2 eV smaller than the VCA result (2.32 eV). This is a consequence of an atomic-scale localization effect (discussed in some detail in Sec. II C).

B. Comparison with experiments

The experimental data are summarized in Table V. At this time, except for a strong low-energy peak corresponding to the Γ-Γ direct transition, the assignments for indirect and pseudodirect transitions are still in dispute. Three major experimental techniques are currently available for detecting the direct transitions: excitation spectra of luminescence, ellipsometry measurements, and resonant Raman scattering.

TABLE V. Experimental data for direct and indirect transition energies in eV. PLE denotes the threshold in excitation spectra of photoluminescence, "Raman" denotes resonant Raman scattering, and PL is the photoluminescence experiment.

	Direct							Indirect			
	PLE		ellipsometry		Raman			PL			Raman
1×1	2.214		2.07		2.006	2.108	1.890	1.931		2.05	1.890
2×2	2.190	2.19	2.08	2.18				1.971	2.070	2.02	
T (K)	2	4.6	RT	30	RT	RT	1.7	2	4.6	4.2	RT
Refs.	52	53	30	53	55	49	37	52	53	25	49

A luminescence excitation experiment[52] at low temperature (2 K) gives the excitation threshold energies at 2.214 eV for the 1×1 lattice and 2.190 eV for the 2×2 lattice, respectively. The recent ellipsometry measurements give $E_0=2.07$ eV (1×1) and $E_0=2.08$ eV (2×2) at room temperature[30] and $E_0=2.18$ eV (2×2) at low temperature.[53] The strong peak for resonant Raman scattering at room temperature for the 1×1 lattice is ranged from 2.006 (Ref. 55) to 2.108 eV.[49] From these data and from the fact that the direct band gaps for GaAs and AlAs are smaller by about 0.1 eV at room temperature, we expect that the direct band gap for the 1×1 lattice is ranged between 2.1 and 2.2 eV. Our calculation gives 2.11 eV for this lattice. The direct band gap for the 2×2 lattice, on the other hand, is well determined to be 2.18–2.19 eV, in good agreement with our calculation 2.18 eV.

The E_1 and E_2 peaks from the ellipsometry measurement[30] are also consistent with the calculated direct transitions at point $\bar{R}$ for the 1×1 lattice, point $\bar{X}$ for the 2×2 lattice, and point $\bar{M}$ for both the 1×1 and 2×2 lattices, i.e., for the 1×1 lattice, $E_1=3.20$ eV, and $E_2=4.67$ eV from experiment, while the calculation predicts $\Delta E_{R(L)}=2.9$ eV and $\Delta E_{M(X)}=4.7$ eV. Similarly, $E_1=3.25$ eV, and $E_2=4.64$ eV compared with $\Delta E_{X(L)}=3.3$ eV and $\Delta E_{M(X)}=4.7$ eV for the 2×2 lattice.

Most data for indirect transitions are measured by photoluminescence experiment performed near zero temperature. These are ranged from 1.89 to 2.05 eV for the 1×1 lattice[25,52,55] and from 1.97 to 2.07 eV for the 2×2 lattice.[25,52,53] A 1.890-eV peak is also observed in the room-temperature Raman-scattering measurement as a weak feature[49] for the 1×1 lattice. Depending on the experimental conditions, these measurements may reveal different features, since the low-energy luminescence peaks corresponding to transitions to the lowest-excited state can be an indirect transition, a pseudodirect transition, a direct transition, or even transitions to defect levels within the energy gap.

The observed luminescence peak for the 1×1 lattice is assigned to the indirect transition to point $\bar{R}$ (1.85 eV). The calculated minimum gap at point $\bar{M}$ for the 2×2 lattice (2.16 eV) is, however, larger than the measured peaks. An alternative assignment in this case is attributed to imperfect growth of the 2×2 lattice, since a local excess of Ga or Al ions can easily create 3×1 (three layers of GaAs and one layer of AlAs) and 1×3 local structures. Our calculation shows that the direct band gap for one of these structures in the ideal form, the perfect 3×1 lattice, is 1.87 eV and is much smaller than the direct band gap for a 2×2 lattice. Hence, whether these local 3×1 structures repeat themselves to form local lattices or exist as local defects, their energy gaps, with the 1.87 eV as the lower bound, are below the direct band gap of the 2×2 lattice and could have been detected by luminescence experiments. The local Al-rich 1×3 structures, on the other hand, have larger direct band gaps and hence could not affect the measurement. Although the probability of forming relatively large local lattices is very low, the transition-matrix elements for direct transitions are, however, much larger than those for indirect transitions. The imperfect growth and the formation of 3×1 and 1×3 local structures could also occur in the 1×1 lattice. In either case, it is unlikely that the measured luminescence peaks should be assigned to transitions to the X_{1c}-derived state at point $\bar{\Gamma}$.

C. Confinements and some microscopic band features

In this subsection, we discuss spatial confinement effects, avoided band crossing, energy oscillation with respect to lattice thickness.

The charge contours for the Γ- and X-derived states at point $\bar{\Gamma}$ up to 3×3 lattice are shown in Fig. 4. The X-derived states qualitatively agree with the Kronig-Penny model in terms of confinement, i.e., as the layer thickness approaches zero, the confinement effects vanish. In contrast, the Γ-derived state is qualitatively different. Some confinement or localization remains in the case of a 1×1 lattice. The more repulsive Al pseudopotentials relative to the Ga pseudopotentials are the cause for the more localization on the GaAs side for the excited states. Because of this localization, the energy for the Γ state for the 1×1 lattice (2.11 eV) is lower than that calculated by the VCA (2.32 eV). A quantitive estimate can be made using the localization percentage listed in Table III. The modified value for this state, $E=2.08$ eV, is in reasonable agreement with the quasiparticle calculation. The cation-potential difference has the maximum effect for the on-site antibonding s-like Γ state and the effect for the interstitial X state is much smaller. We suggest that this localization at atomic scale also causes the observed largest bowing effect for the Γ state in Ga(Al)-As alloys, i.e., the point Γ gap for $Ga_{0.5}Al_{0.5}As$ alloy is about 0.1–0.15 eV (Refs. 62 and 63) smaller than the VCA gap.

The quasiparticle energy order at point $\bar{\Gamma}$ for the 1×1 lattice indicates band crossings. An avoided crossing occurs between the two lowest conduction bands along line Λ (from point Γ to point $\bar{Z}$) near 10% off the zone center [see part (a) of Fig. 5]. Another avoided crossing

occurs between the second and the third lowest conduction bands near 30% off the zone center in the same direction. There are two important consequences. (1) The longitudinal effective mass for the $\bar{\Gamma}_4(X)$ state is about 70% smaller than the corresponding effective mass of GaAs (or AlAs) at X minima so that the $\bar{\Gamma}_4$ valley is nearly spherically symmetric. $m_l(\bar{\Gamma}_4)=0.23m_0$ and $m_t(\bar{\Gamma}_4)=0.21m_0$, where m_0 is the free-electron mass. This reduced effective mass also reduces the optical-transition probability for transitions to this state since the density of states near point $\bar{\Gamma}_{4c}$ is reduced; (2) large variations of the optical-transition matrix elements as a function of wave vector $\mathbf{k}_z$ are expected.

We have calculated the relevant matrix elements, $|\langle\psi_i|\mathbf{p}|\psi_f\rangle|^2$, for transitions from the upper valence bands to the lower conduction bands near the zone center.[64] Results are shown in part (b) of Fig. 5. The lower of the zone-folded states ($\bar{\Gamma}_{4c}$) does not mix with the Γ-derived point $\bar{\Gamma}_{1c}$ by symmetry so the matrix element is essentially zero. The second zone-folded state has a significant oscillator strength. The situation reverses for the 2×2 lattice. However, the matrix element is further reduced by the spatial separation of the electrons and holes, being about 0.01 a.u. (compared to 0.25 a.u. for Γ_{1c}-derived level). Moving away from the zone center, there is a significant anisotropy in the matrix elements that derives from the anticrossing behavior in the $\mathbf{k}_z$ direction, which is illustrated in part (a) of Fig. 5. As the avoided crossing is approached, the $\bar{\Gamma}_{1c}$- and $\bar{\Gamma}_{4c}$-derived bands exhibit strong mixing. The oscillator

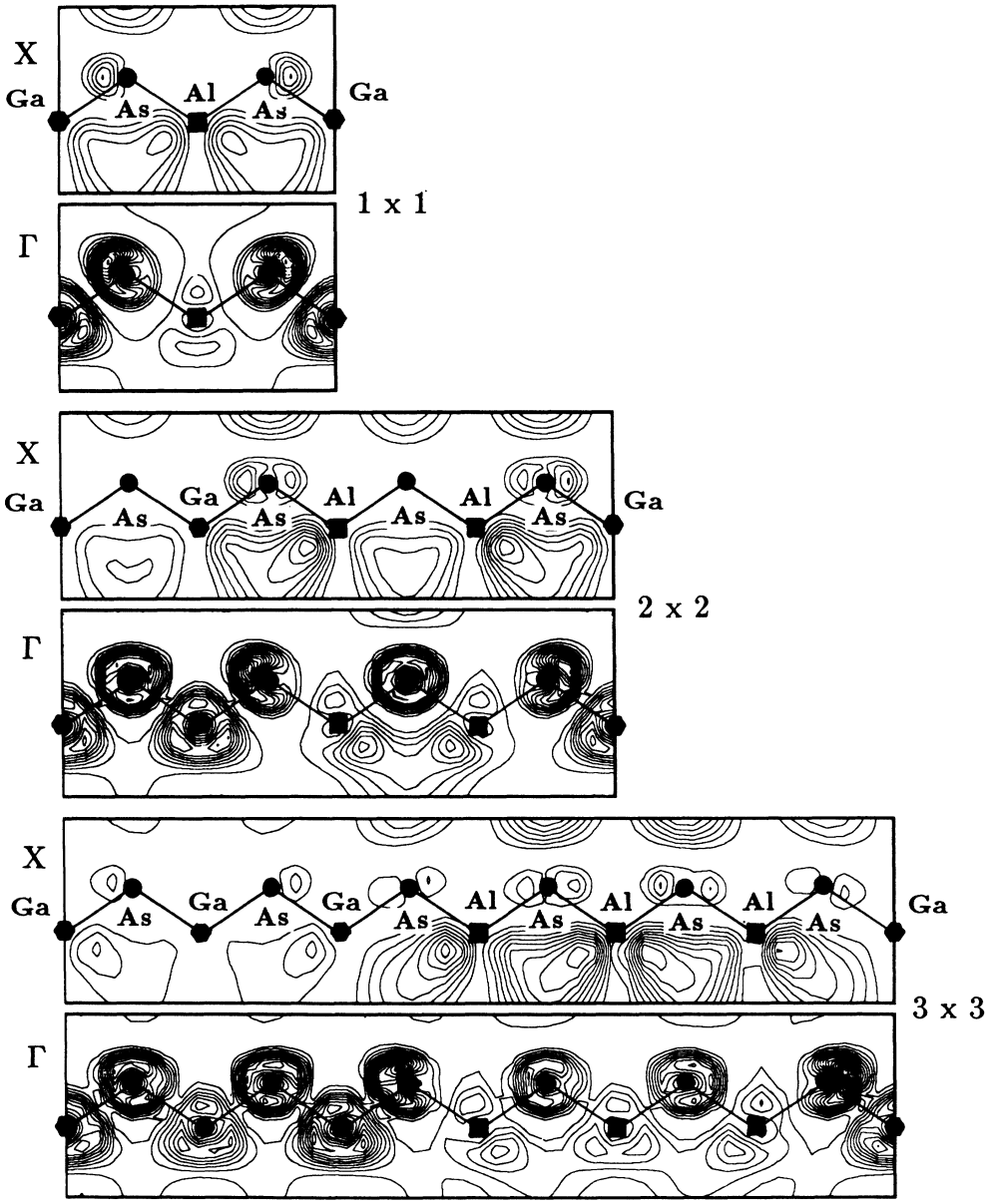

FIG. 4. Charge-density contours in the $(10\bar{1})$ plane for the low-lying Γ- and X-derived conduction-band states for the 1×1, 2×2, and 3×3 superlattices.

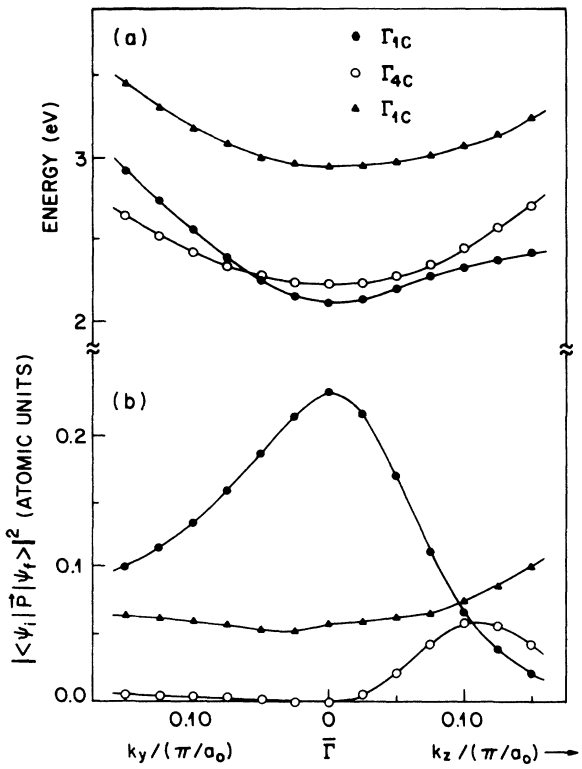

FIG. 5. Calculated (a) quasiparticle conduction-band energies, and (b) optical matrix elements squared, near the zone center for the 1×1 lattice.

strength is transferred from the lower to the upper band. In the perpendicular direction, where no avoided crossing occurs, the oscillator strength for the $\bar{\Gamma}_{1c}$-derived band drops smoothly and the zone-folded band has very little oscillator strength.

In principle, the spin-orbit interaction can mix states of different symmetries. Our calculation, however, showed that this does not affect the matrix elements significantly, e.g., with the spin-orbit coupling, the matrix-element square for transitions to the $\bar{\Gamma}_{4c}$ state for the 1×1 lattice is still very small, about 4 orders of magnitude smaller than that for transitions to the $\bar{\Gamma}_{1c}$ state. The spin-orbit results are summarized in Table VI. These transitions are polarized. For example, the z component $|\langle\psi_i|p_z|\psi_f\rangle|^2$ is zero for transitions from the planarlike valence $\bar{\Gamma}_{5v}$ states to the s-like Γ conduction state. In contrast, transitions from $\bar{\Gamma}_{5v}$- to the X_{1c}-derived state are polarized in the z direction. Although the anisotropies have not been observed for ultrathin superlattices, polarization studies for GaAs-AlGaAs quantum wells[65] are consistent with our calculations. The matrix elements for infrared transition between the two conduction states are also significant.

TABLE VI. Transition-matrix elements for the 1×1 GaAs/AlAs lattice calculated with spin-orbit interaction in Rydberg atomic units. m_j is the quantum number of the z component of total angular momentum j.

$i\rightarrow f$	δm_j	$\lvert\langle\psi_i\lvert\mathbf{p}\rvert\psi_f\rangle\rvert^2$	$\lvert\langle\psi_i\lvert p_z\rvert\psi_f\rangle\rvert^2$
$\bar{\Gamma}_{5v}\rightarrow\bar{\Gamma}_{1c}$	even	0.02	0.0
	odd	0.22	0.0
$\bar{\Gamma}_{4v}\rightarrow\bar{\Gamma}_{1c}$	even	0.06	0.01
	odd	0.17	0.16
$\bar{\Gamma}_{5v}\rightarrow\bar{\Gamma}_{4c}$	even	0.30×10^{-5}	~0
	odd	$0.19\times10.^{-4}$	0.19×10^{-4}
$\bar{\Gamma}_{4v}\rightarrow\bar{\Gamma}_{4c}$	even	0.26×10^{-5}	0.0
	odd	0.27×10^{-4}	0.0
$\bar{\Gamma}_{1c}\rightarrow\bar{\Gamma}_{4c}$	even	0.19×10^{-2}	0.19×10^{-2}
	odd	0.18×10^{-1}	0.18×10^{-1}

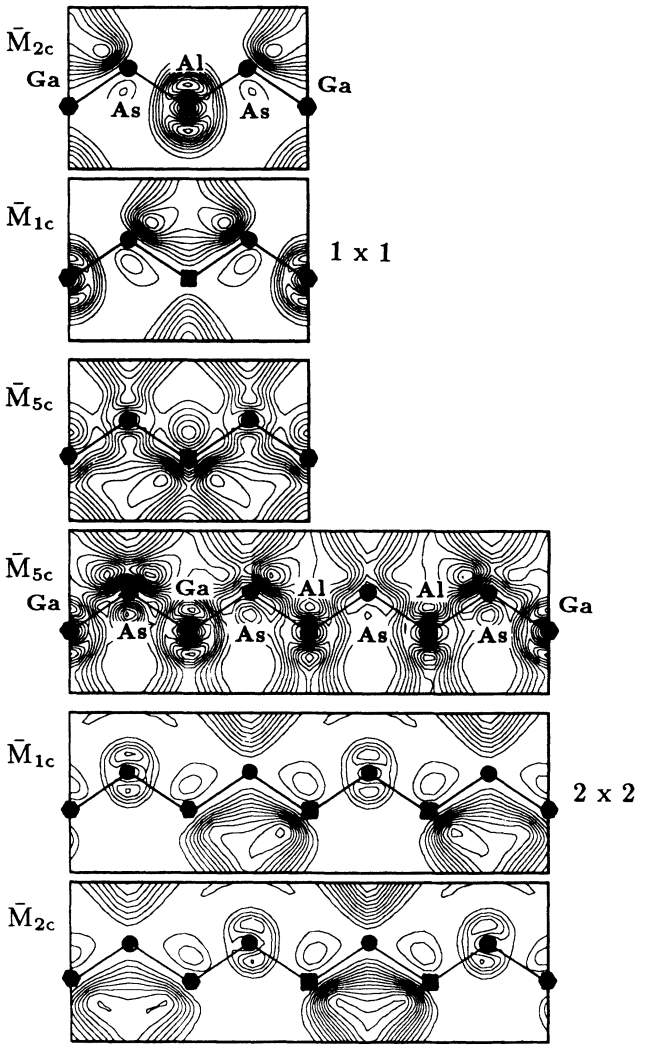

FIG. 6. Charge-density contours in the $(10\bar{1})$ plane. The points $\bar{M}_{2c}$ and $\bar{M}_{1c}$ are the segregating states, and the point $\bar{M}_{5c}$ is the degenerate states of the 1×1 lattice; the point $\bar{M}_{5c}$ is the degenerate states, and the points $\bar{M}_{1c}$ and $\bar{M}_{2c}$ are the segregating states for the 2×2 lattice. Charge densities for the degenerate states are symmetrized.

The minimal rectangular unit cell of the zinc-blende structure along the [001] direction contains twice the volume of its primitive cell and two chemical formulas. The two molecular sites provide two natural registries for segregation of paired states, which are derived from degenerate bulk states. For a superlattice with an even number of sublayers, 2×2, 4×4, etc., each subcell of GaAs or AlAs also contains a multiple of such mini (rectangular)-cells. This condition, on the other hand, cannot be satisfied by superlattices with odd numbers of sublayers, 1×1, 3×3, etc., and in this case one of the minicell is shared by one GaAs and one AlAs molecule. The commensuration and incommensuration between the minicell and the subcells of GaAs and AlAs for (001) superlattice cause the energy oscillations for the paired states at points $\bar{M}$ and $\bar{R}(\bar{X})$ [see Figs. 3(a) and 3(b)].

An example is the paired X_{3c} states with charge residents in the cation layers (the points $\bar{M}_{1c}$ and $\bar{M}_{2c}$ for the 1×1 lattice and the corresponding point $\bar{M}_{5c}$ for the 2×2 lattice shown in Fig. 6). These states segregate for odd number of sublayers. The energy separation is sizable because it reflects the on-site potential difference between Ga and Al ions. For an even number of sublayers, however, the minicell commensurate with the subcells and the two registries within the minicell are equivalent causing degeneracy. Another example is the paired X_{1c} states. These states form superlattice states with charge residing on the common-anion As layers. For this pair of states, segregation may occur because there are two interfacial As sites in each supercell. Degeneracy occurs for odd number of sublayers since, in this case, the minicell incommensurates with the subcells and this forces each state to occupy both interfacial As sites. In the even number case, the energy separation between this pair reflects the nearest-neighbor cation-potential difference and is hence smaller. The repulsion between the X_1 states was once suggested as the cause for a lower $\bar{M}(X_{1c,xy})$ level relative to the $\bar{\Gamma}(X_{1c,z})$ level.[59] This does not apply because the repulsion vanishes for odd-sublattice periods.

IV. SUMMARY

We have calculated (1) the valence-band offset for GaAs/AlAs (001) with quasiparticle many-body corrections. These corrections are dominated by many-body contributions to the bulk eigenenergies. Our result is in better agreement with experiment than the LDA result, which demonstrates the limitation of the current LDA scheme. (2) The electronic structures of GaAs/AlAs (001) ultrathin superlattices were determined. The effects of many-body interactions and atomic-scale localization on superlattices were also examined. We found that, due to these effects, the 1×1 and 2×2 lattices have direct band gaps instead of pseudodirect band gaps at point $\bar{\Gamma}$. Available experimental data are consistent with the theory.

ACKNOWLEDGMENTS

The work at Berkeley was supported by National Science Foundation (under Grant No. DMR-88-18404) and by the Director, Office of Energy Research (Materials Sciences Division of the Office of Basic Energy Sciences), U.S. Department of Energy (under Contract No. DE-AC03-76SF00098). D.T. was supported by the Center for Advanced Materials at the Lawrence Berkeley Laboratory. M.L.C. acknowledges support from the Miller Institute for Basic Research in Science and S.G.L. acknowledges support from the John Simon Guggenheim Memorial Foundation. Cray computer time was provided by the NSF San Diego Supercomputer Center.

*Present address: Xerox Corporation, Palo Alto Research Center, 3333 Coyote Hill Road, Palo Alto, CA 94304.

†Present address: Department of Physics and Astronomy and Center for Fundamental Materials Research, Michigan State University, East Lansing, MI 48824-1116.

[1]See, for example, Proceedings of the 12th Annual Conference on the Physics and Chemistry of Semiconductor Interfaces, Tempe, Arizona, 1985 [J. Vac. Sci. Technol. B **3**, (1985)] for general reviews.

[2]R. S. Bauer and G. Margaritondo, Phys. Today **40**, No. 1, 27 (1987).

[3]H. Kroemer, J. Vac. Sci. Technol B **2**, 433 (1984).

[4]G. Duggan, J. Vac. Sci. Technol. B **3**, 1224 (1985).

[5]R. Dingle, W. Wiegmann, and C. H. Henry, Phys. Rev. Lett. **33**, 827 (1974).

[6]J. O. McCaldin, T. C. McGill, and C. A. Mead, Phys. Rev. Lett. **36**, 56 (1976).

[7]R. C. Miller, D. A. Kleinman, and A. C. Gossard, Phys. Rev. B **29**, 7085 (1984).

[8]R. L. Anderson, Solid State Electron. **5**, 341 (1962).

[9]W. A. Harrison, J. Vac. Sci. Technol. **14**, 1016 (1977).

[10]W. R. Frensley and H. Kroemer, Phys. Rev. B **16**, 2642 (1977).

[11]W. I. Wang and F. Stern, J. Vac. Sci. Technol. B. **3**, 1280 (1985).

[12]J. Batey and S. L. Wright, J. Appl. Phys. **59**, 200 (1986).

[13]J. Menéndez, A. Pinczuk, D. J. Werder, A. C. Gossard, and J. H. English, Phys. Rev. B **33**, 8863 (1986).

[14]P. Dawson, K. J. Moore and C. T. Foxon, Proc. SPIE **792**, 208 (1987).

[15]D. J. Wolford, in *Proceedings of the 18th International Conference on the Physics of Semiconductors, Stockholm (1986)*, edited by O. Engström (World Scientific, Singpore, 1987), pp. 1115; and private communication.

[16]W. E. Pickett, S. G. Louie, and M. L. Cohen, Phys. Rev. B **17**, 815 (1978).

[17]J. Tersoff, Phys. Rev. B **30**, 4874 (1984).

[18]C. G. Van de Walle and R. M. Martin, J. Vac. Sci. Technol. B **4**, 1055 (1986).

[19]S. Massidda, B. I. Min, and A. J. Freeman, Phys. Rev. B **35**, 9871 (1987).

[20]S. H. Wei and A. Zunger, Phys. Rev. let **59**, 144 (1987).

[21]D. M. Bylander and L. Kleinman, Phys. Rev. B **36**, 3229 (1987).

[22]S. B. Zhang, D. Tománek, S. G. Louie, M. L. Cohen, and M. S. Hybertsen, Solid State Commun. **66**, 585 (1988).
[23]The *d* core relaxation effect is expected to be less than 0.05 eV for the present case (see Ref. 22).
[24]P. M. Petroff, Nature (London) **316**, 389 (1985).
[25]A. Ishibashi, Y. Mori, M. Itabashi, and M. Watanabe, J. Appl. Phys. **58**, 2691 (1985).
[26]G. Danan, B. Etienne, F. Mollot, R. Planel, A. M. Jean-Louis, F. Alexandre, B. Jusserand, G. Le Roux, J. Y. Marzin, H. Savary, and B. Sermage, Phys. Rev. B **35**, 6207 (1987).
[27]G. Bastard, Phys. Rev. B **24**, 5693 (1981).
[28]D. M. Wood, S. H. Wei, and A. Zunger, Phys. Rev. B **37**, 1342 (1988).
[29]S. H. Wei and A. Zunger, J. Appl. Phys. **63**, 5794 (1988).
[30]M. Alouani, S. Gopalan, M. Garriga, and N. E. Christensen, Phys. Rev. Lett. **61**, 1643 (1988).
[31]S. Gopalan, N. E. Christensen, and M. Cardona, Phys. Rev. B **39**, 5165 (1989).
[32]D. M. Bylander and L. Kleinman, Phys. Rev. B **34**, 5280 (1986).
[33]M. Posternak, A. Baldereschi, S. Massidda, and A. J. Freeman, in *Proceedings of 14th International Symposium on GaAs and Related Compounds, Heraklion, Crete, Greece, 1987,* Inst. Phys. Conf. Ser. No. 91, edited by A. Christou and H. S. Rupprecht (IOP, Bristol, 1988), p. 537.
[34]I. P. Batra, S. Ciraci, and J. S. Nelson, J. Vac. Sci. Technol. B **5**, 1300 (1987).
[35]S. Ciraci and I. P. Batra, Phys. Rev. Lett. **58**, 2114 (1987).
[36]B. I. Min, S. Massidda, and A. J. Freeman, Phys. Rev. B **38**, 1970 (1988).
[37]E. Finkman, M. D. Sturge, and M. C. Tamargo, Appl. Phys. Lett. **49**, 1299 (1986).
[38]M. H. Meynadier, R. E. Nahory, J. M. Worlock, M. C. Tamargo, J. L. de Miguel, and M. D. Sturge, Phys. Rev. Lett. **60**, 1338 (1988).
[39]E. Finkman, M. D. Sturge, M. H. Meynadier, R. E. Nahory, M. C. Tamargo, D. M. Hwang, and C. C. Chang, J. Lumin. **39**, 57 (1987).
[40]G. Duggan, H. I. Ralph, P. Dawson, K. J. Moore, C. T. B. Foxon, R. J. Nicholas, J. Singleton, and D. C. Rogers, Phys. Rev. B **35**, 7784 (1987).
[41]M. S. Hybertsen and S. G. Louie, Comments Condens. Matter Phys. **13**, 223 (1987), and references therein.
[42]M. S. Hybertsen and S. G. Louie, Phys. Rev. B **34**, 5390 (1986).
[43]S. B. Zhang, D. Tománek, M. L. Cohen, S. G. Louie, and M. S. Hybertsen, Phys. Rev. B **40**, 3162 (1989).
[44]C. G. Van de Walle and R. M. Martin, J. Vac. Sci. Technol. B **3**, 1256 (1985).
[45]Landolt-Börnstein, *Numerical Data and Functional Relationships in Science and Technology—Crystal and Solid State Physics,* edited by O. Madelung (Springer, Berlin, 1984), Vol. 17a.
[46]We emphasize the importance of sampling the three-dimensional Brillouin zone in superlattice calculations. In the present case, two layers of **k** points along the *z* direction have been used in the Brillouin-zone sum. The in-plane components k_x and k_y correspond exactly to the two-dimensional special set of 3 **k** points [S. L. Cunningham, Phys. Rev. B **10**, 4988 (1974)].
[47]A. Baldereschi, S. Baroni, and R. Resta, Phys. Rev. Lett. **61**, 734 (1988).
[48]E. Caruthers and P. J. Lin-Chung, Phys. Rev. Lett. **38**, 1543 (1977).
[49]M. Cardona, T. Suemoto, N. E. Christensen, T. Isu, and K. Ploog, Phys. Rev. B **36**, 5906 (1987).
[50]W. Andreoni and R. Car, Phys. Rev. B **21**, 3334 (1980).
[51]T. Isu, D. S. Jiang, and K. Ploog, Appl. Phys. A **43**, 75 (1987).
[52]D. S. Jiang, K. Kelting, T. Isu, H. J. Queisser, and K. Ploog, J. Appl. Phys. **63**, 845 (1988).
[53]J. Nagle, M. Garriga, W. Stolz, T. Isu, and K. Ploog, J. Phys. (Paris) Colloq. **48**, C5-495 (1987).
[54]M. Garriga, M. Cardona, N. E. Christensen, P. Lautenschlager, T. Isu, and K. Ploog, Phys. Rev. B **36**, 3254 (1987).
[55]N. Kobayashi, T. Toriyama, and Y. Horikoshi, Appl. Phys. Lett. **50**, 1811 (1987).
[56]J. N. Schulman and T. C. McGill, Phys. Rev. B **19**, 6341 (1979).
[57]T. Nakayama and H. Kamimura, J. Phys. Soc. Jpn. **54**, 4726 (1985).
[58]J. Ihm, Appl. Phys. Lett. **50**, 1068 (1987).
[59]M. A. Gell, D. Ninno, M. Jaros, and D. C. Herbert, Phys. Rev. B **34**, 2416 (1986).
[60]J. Menédez, A. Pinczuk, J. P. Valladares, L. N. Pfeiffer, K. W. West, A. C. Gossard, and J. E. English (unpublished).
[61]The energy gap at point L_{1c} for AlAs has not been directly measured (Refs. 62 and 63). Hence, no correction is made for this case.
[62]R. W. Godby, M. Schlüter, and L. J. Sham, Phys. Rev. B **35**, 4170 (1987).
[63]D. E. Aspnes, S. M. Kelso, R. A. Logan, and R. Bhatt, J. Appl. Phys. **60**, 754 (1986).
[64]The precise value is somewhat uncertain as the LDA wave functions are used to calculate the matrix elements and the self-energy calculation places the avoided crossing at a slightly different point in **k** space.
[65]J. E. Zucker, A. Pinczuk, D. S. Chemla, A. Gossard, and W. Wiegmann, in *Proceedings of the 17th International Conferences on Physics of Semiconductors, San Francisco, 1984* (Springer-Verlag, New York, 1985), p. 563.